Radiological and non-radiological leaching assessment of alkali-activated materials containing ground granulated blast furnace slag and phosphogypsum

Peer-reviewed author version

GIJBELS, Katrijn; Landsberger, Sheldon; SAMYN, Pieter; Iacobescu, Remus Ion; Pontikes, Yiannis; SCHREURS, Sonja & SCHROEYERS, Wouter (2019)
Radiological and non-radiological leaching assessment of alkali-activated materials containing ground granulated blast furnace slag and phosphogypsum. In: Science of the total environment, 660, p. 1098-1107.

DOI: 10.1016/j.scitotenv.2019.01.089
Handle: http://hdl.handle.net/1942/28168

RADIOLOGICAL AND NON-RADIOLOGICAL LEACHING ASSESSMENT OF ALKALI-ACTIVATED MATERIALS CONTAINING GROUND GRANULATED BLAST FURNACE SLAG AND PHOSPHOGYPSUM

Katrijn GIJBELS[a*], Sheldon LANDSBERGER[b], Pieter SAMYN[c], Remus Ion IACOBESCU[d], Yiannis PONTIKES[d], Sonja SCHREURS[a], Wouter SCHROEYERS[a]

[a] Hasselt University, CMK, Nuclear Technological Centre, Agoralaan, Gebouw H, 3590 Diepenbeek, Belgium

[b] Nuclear Engineering Teaching Lab, University of Texas at Austin, Pickle Research Campus, Austin, TX 78712, USA

[c] Hasselt University, IMO, Applied and Analytical Chemistry, Agoralaan, Gebouw D, 3590 Diepenbeek, Belgium

[d] KU Leuven, Department of Materials Engineering, Kasteelpark Arenberg 44, 3001 Leuven, Belgium

* Corresponding author: Katrijn GIJBELS, +3211292157 (Tel.), +3211268199 (Fax.)

katrijn.gijbels@uhasselt.be, s.landsberger@mail.utexas.edu, pieter.samyn@uhasselt.be, remusion.iacobescu@kuleuven.be, yiannis.pontikes@kuleuven.be, sonja.schreurs@uhasselt.be, wouter.schroeyers@uhasselt.be

Abstract

Alkali-activated materials (AAMs) based on ground granulated blast furnace slag (GGBFS) and phosphogypsum (PG) were investigated in order to quantify leaching of naturally occurring radionuclides (NOR) and inorganic non-radiological elements according to an up-flow percolation column test as described in CEN/TS 16637-3. Gamma spectroscopy and neutron activation analysis (NAA) were applied for radiological characterization, inductively coupled plasma optical emission spectrometry (ICP-OES) and ion-chromatography (IC) for chemical characterization. Upon leaching, ^{238}U, ^{226}Ra, ^{210}Pb, and ^{228}Ra were retained very well. Both for ^{232}Th and ^{40}K, a decrease in activity concentration was observed due to leaching and their release was influenced by the use of different alkali activators, which was also the case for the leaching of non-radiological elements. Only a small amount of Al (0.5-0.8%), Ca (0.1-0.2%) and Si (0.1-0.3%) was mobilized, while highest release was observed for K (56-94%), Na (49-88%) and S (71-87%). At first glance, drinking water is not endangered by leaching of NOR following the requirements of the European Drinking Water Directive. From the results for porosity, obtained with mercury intrusion porosimetry (MIP), it was concluded that both the porosity and formation of multiple leachable and non-leachable complexes are determining factors for the release of elements from AAMs.

Keywords

Alkali-activated material, ground granulated blast furnace slag, phosphogypsum, naturally occurring radionuclides, leaching

1. Introduction

From a sustainability perspective, the reuse of industrial by-products or residues in the production of construction materials has become an indispensable practice to reduce waste production, CO_2

emissions, energy and natural resources usage by replacement of primary raw materials. In this respect, Ordinary Portland Cement (OPC) can be replaced by alkali-activated materials (AAMs), which are considered as promising alternative binders due to (1) their excellent performance characteristics, and (2) because they can be synthesized from by-products or residues (Provis, 2017). However, by-products or residues can be characterized by enhanced concentrations of hazardous compounds, such as heavy metals and/or naturally occurring radionuclides (NOR) (Nuccetelli et al., 2015). Therefore, AAMs must be capable to immobilize these particular compounds, starting from the use scenario as well as during demolition, recycling and disposal (end-of-life). Hence in the evaluation of AAMs, the whole life-cycle must be considered.

This study describes the incorporation of phosphogypsum (PG) in AAMs based on ground granulated blast furnace slag (GGBFS). PG originates from the phosphate industry, where phosphoric acid is separated from phosphate ore by treatment with sulphuric acid. PG is characterized by enhanced levels of NOR, mainly from the ^{238}U series, provoking many restrictions on its use. Besides, impurities such as P_2O_5, F^-, organic substances and alkali metals can be incorporated (Tayibi et al., 2009; Wang et al., 2018). PG is disposed of in large stockpiles, occupying vast areas of land which is very costly due to mandatory environmental monitoring and long-term maintenance (Central Pollution Control Board, 2012; Tayibi et al., 2009). Up to 2006, the total amount of PG produced worldwide is estimated to have been about 6 billion tons (International Atomic Energy Agency (IAEA), 2013), consequently large-scale valorization options are needed to consume these vast amounts (Rashad, 2017). GGBFS has already been extensively studied for the production of AAMs, being an excellent precursor for alkali activation and allowing the incorporation of precursors which are less suitable, such as PG (Kuo et al., 2014; Lancellotti et al., 2018; Ulubeyli and Artir, 2015). PG participates as an additional source of sulphate, giving rise to additional reaction products compared to AAMs solely based on slags (Nguyen et al., 2018). The levels of NOR in GGBFS are low, consisting of radionuclides from both the ^{238}U and ^{232}Th series (Sas et al., 2017).

Concerning NOR in building materials, the European Basis Safety Standards (EU-BSS) Directive (Council Directive 2013/59/Euratom) sets down a framework for screening of gamma exposure from building materials. In addition to outdoor external exposure, the reference level for indoor external exposure emitted by building materials is set at 1 mSv/y (Council of the European Union, 2014). This aspect has been described in detail in a complementary study (Gijbels et al., 2018). Nonetheless, less attention has been paid to the leaching behavior of NOR from building materials (Croymans et al., 2017; Michalik et al., 2018; Mossini et al., 2015). Consequently, there is poor understanding of the potential migration of NOR, especially in the alkaline range of pH, which is the main condition imposed by AAMs. Notwithstanding, reuse of naturally occurring radioactive materials (NORM), such as PG, in building materials may lead to leaching of NOR to groundwater and can consequently affect the quality of drinking water supplies, which could be a concern from the radiation protection point of view (Contreras et al., 2014, 2013). AAMs are often used for stabilization/solidification purposes (Huang et al., 2017; Shi and Fernández-Jiménez, 2006) and consequently low leaching rates are expected. A detailed investigation of NOR leaching is lacking and is presented in this study, aiming to prevent anthropogenic influence on the environment, in particular the contamination of water. Leaching of non-radiological elements (e.g. calcium or sodium) can possess synergistic effects on NOR leaching and should be studied in parallel.

Leaching of inorganic constituents from building materials can be assessed either by batch or column leaching tests (Hjelmar et al., 2012; Nebel and Spanka, 2013). Batch tests may underestimate the actual release of contaminants, while column tests provide more reliable field-correlated information (Cappuyns and Swennen, 2008). Moreover, the release behavior during the end-of-life phases of the building material is more accurately predicted when compared to batch tests.

The radioactivity of the ^{238}U and ^{232}Th isotope decay chains in processed industrial by-products or residues, such as GGBFS and PG, are mostly characterized to be in disequilibrium resulting in differences in the activity concentration for the radionuclides of a given decay chain (Michalik et al.,

2018). For this reason, assessment of leaching requires careful evaluation. Only NOR with a half-life long enough to behave independently in the environment will be considered in the leaching assessment (Michalik et al., 2018).

The overall goal of the present study is to assess the leaching of NOR (more specific the long-lived radionuclides from these natural decay chains, and ^{40}K) and non-radiological elements from AAMs based on GGBFS when PG is incorporated. In a conservative approach, the requirements set by the European Drinking Water Directive are used for the evaluation of NOR leaching from AAMs (Council of the European Union, 2013). Also the influence of alkaline solution on leaching and porosity is assessed. In a complementary study, the maximum amount of PG which can be incorporated following the EU-BSS requirements, was determined (Gijbels et al., 2018).

2. Experimental

2.1 Materials

A combination of GGBFS and PG was used as precursor. GGBFS was provided by a Belgian steel company. It was dried in a laboratory oven at 110 °C and subsequently milled to a Blaine fineness of 4050 ± 200 cm^2/g, determined according to EN 196-6 (Bureau voor Normalisatie (NBN), 2010). The density of GGBFS was found to be 2.9 g/cm^3 (Quantachrome Multipycnometer MVP-6DC) according to ASTM C204 (ASTM International, 2017). The chemical composition of GGBFS, determined by X-ray fluorescence analysis (Philips, PW 1830), was (in wt%): 36.2 ± 0.2 SiO_2, 40.3 ± 0.5 CaO, 11.4 ± 0.2 Al_2O_3, 8.2 ± 0.1 MgO, 1.1 ± 0.1 S, 0.8 ± 0.1 TiO_2, 0.8 ± 0.1 Na_2O, 0.5 ± 0.1 K_2O and 0.3 ± 0.1 FeO. PG was derived from the International Atomic Energy Agency (IAEA) (reference material 434) (Shakhashiro et al., 2011) and was used as received with particle size ranging from 0.5 µm to 30 µm. The matrix composition of PG was provided by the supplier and consisted of (in wt%): 96 $CaSO_4.2H_2O$, 1-2 P_2O_5, 1.2 F, 1 SiO_2 and 0.2 Al_2O_3. The sodium silicate solution used in the experiments was supplied by ABCR GmbH (molar ratio SiO_2/Na_2O = 3.3 and 65% water). Sodium

hydroxide pellets (99% purity) were purchased from Chem-Lab. Distilled water (ASTM type II) was used throughout the experiments.

2.2 Sample synthesis

Sodium silicate solution was mixed with sodium hydroxide pellets and distilled water to form an alkaline solution with three different molar ratios (SiO_2/Na_2O=0.75 and H_2O/Na_2O=20, SiO_2/Na_2O=0 and H_2O/Na_2O=27.8, SiO_2/Na_2O=0 and H_2O/Na_2O=18.5). The alkaline solutions were then left overnight to cool to ambient temperature.

Samples were prepared with a GGBFS/PG mass ratio of 9/1 and the mass ratio between the alkaline solution and dry mix (GGBFS + PG) was 3/5. GGBFS and PG were mixed thoroughly until a uniform blend was produced. The alkaline solution was then stirred for 3 min with the dry mix to form a homogeneous paste. The pastes were cast in polymer coated steel molds (20 mm x 20 mm x 80 mm) and allowed to consolidate for 24 h at room temperature having the molds wrapped with plastic foil to avoid water evaporation. After 24 h, the samples were demolded and were stored in sealed storage vessels for further curing at room temperature till they were 28 days old. Table 1 gives an overview of the sample compositions, which were selected for their compressive strength at 28 days (tested in a previous study (Gijbels et al., 2018) and presented in Table 1).

Table 1: Composition of the samples

Sample	SiO_2/Na_2O	H_2O/Na_2O	wt% GGBFS	wt% PG	Alkaline solution/dry mix	Compressive strength (MPa)
Sample 1	0.75	20.0	90	10	0.6	52.8
Sample 2	0	27.8	90	10	0.6	16.0
Sample 3	0	18.5	90	10	0.6	22.3

2.3 Leaching test

The leaching of non-volatile inorganic NOR and non-radiological elements as a function of liquid-over-solid ratio (L/S) was assessed by means of an up-flow percolation test as described in CEN/TS 16637-3 (European Committee for Standardization, 2016). After a curing period of 28 days, samples were dried in a laboratory oven at 40 °C till constant mass, whereafter they were cooled down in a desiccator. Subsequently, samples were crushed till 45% by mass of the test sample had a particle size lower than 4 mm, while 100% by mass had a particle size lower than 16 mm. For the leaching test, 90 g of sample was placed in a column made of glass with an inner diameter of 30 mm and a length of 200 mm. In the top and bottom of the column, a filter paper (Schleicher & Schuell, nr. 595) was fixed, and the outlets were connected with Viton® tubing material with an inner diameter of 1.6 mm. A volumetric peristaltic pump (SP100 OEM fixed flow peristaltic pump, APT Instruments) pumped the leachant through the setup with a flow rate of 0.096 ml/min. Distilled water was used as leachant solution to allow a rapid screening of potentially leachable elements and the results are independent of variable local surface, ground- and rainwater chemistry. A saturation period of 20 h was applied whereafter 7 eluate fractions were collected at predefined intervals (0.10 ± 0.02 l/kg, 0.10 ± 0.02 l/kg, 0.30 ± 0.05 l/kg, 0.50 ± 0.05 l/kg, 1.00 ± 0.05 l/kg, 3.0 ± 0.1 l/kg, 5.0 ± 0.2 l/kg) until a cumulative L/S of 10.0 ± 0.5 l/kg was reached. The bottles for collection of the eluates were covered with film in order to minimize carbonation. Due to their small volume, the first 2 eluate fractions were diluted by a factor 2. The pH (HI2211 pH/ORP Meter, HANNA Instruments) and conductivity (Konduktometer CG 858, Schott Geräte) of each eluate fraction was measured immediately after collection. Leaching tests were done under laboratory conditions (temperature 20 ± 2 °C, relative humidity about 50%). Between each leaching test, the set-up was first rinsed with diluted (0.1 mol/l) nitric acid (65%, supplied by Merck) and thereafter with distilled water. After leaching, the samples were dried in a laboratory oven at 100 °C till constant mass.

166 **2.4 Analysis procedure for naturally occurring radionuclides**

167 For the analysis of NOR, samples were radiometrically counted before (A_0) (in Bq/kg dry mass) and
168 after (A_f) (in Bq/kg dry mass) leaching, and the release is calculated with Eq. 1:

169 $$Release\ (\%) = \left[\frac{A_0 - A_f}{A_0}\right] x\ 100\ \ (Eq.\ 1)$$

170 For the analysis of ^{226}Ra, ^{210}Pb, ^{228}Ra and ^{40}K, samples were gamma spectroscopically counted (A_0)
171 after enclosing radon-tight in a sealed cylindrical polystyrene container of 55 mm diameter and 105
172 mm height for 30 days to reach secular equilibrium of the progenies. Samples were measured on top
173 of a hyper-pure germanium (HPGe) detector (Mirion Technologies (Canberra) model BE5075-7500SI).
174 Shielding against the background radiation was achieved by 0.2 cm copper and 10 cm lead. The
175 system was calibrated with respect to energy using standard sources. The relative efficiency of the
176 detector is 48%, and its energy resolution is 0.346, 0.587 and 1.768 at full width half maximum
177 (FWHM) from 5.9 keV, 122 keV and 1332.5 keV, respectively. The efficiency (ε) as a function of the
178 gamma energy (in keV) was determined using Canberra Laboratory Sourceless Calibration software
179 (LabSOCS) by loading the geometry dimensions, mass, shape, material composition and detector
180 configuration and position for each measurement setup. The data and spectra were recorded by a
181 Lynx MCA. The sample measuring time was 67 h. The background spectrum measured under the
182 same conditions with an empty sealed beaker was used to correct the net peak area of measured
183 gamma rays from the samples. The activities were calculated by the software program Genie 2000
184 from Canberra. The activity of ^{226}Ra and progeny was estimated from the full energy peaks of ^{214}Bi
185 (609.3 keV, 1120.3 keV, 1729.6 keV and 1764.5 keV) and ^{214}Pb (351.9 keV). The activity of ^{210}Pb is
186 determined by its 46.5 keV full energy peak. The activity of ^{228}Ra was estimated by the 911.2 keV full
187 energy peak of ^{228}Ac. The ^{40}K activity concentration was estimated using its 1460.8 keV gamma peak.
188 After leaching and drying, samples were enclosed again for 30 days, whereafter they were counted
189 (A_f) again with the same procedure as for A_0.

For the analysis of ^{238}U and ^{232}Th, thermal and epithermal neutron activation analysis (NAA) was chosen for determination of A_0 and A_f. Before and after leaching, 3 g of the dried sample was separated, homogenized with a mortar and passed through a 250 micron filter. Thereafter, the sample was placed in a polyethylene container. ^{238}U was determined using epithermal neutrons with a neutron flux of ~2.25 x 10^{12} n cm^2/s for an irradiation time of 2 min at 500 kW with a decay time of 10 min and a counting time of 5 min. For analysis of ^{232}Th, thermal neutrons were used with a neutron flux of ~4.5 x 10^{12} n cm^2/s and irradiated for 3 h at 950 kW with a decay time of 2 weeks and a counting time of 4 h. All neutron irradiations were performed using the TRIGA MARK II 1.1 MW reactor at the Nuclear Engineering Teaching Lab (University of Texas). A description of the experimental conditions is shown in Table 2. ^{238}U was determined by the 74.5 keV gamma-ray of ^{239}U ($t_{1/2}$ = 25 min) and ^{232}Th by the 311.9 keV gamma-ray of ^{233}Pa ($t_{1/2}$ = 27.7 days) with a HPGe ORTEC detector with a FWHM of 2.1 keV gamma-ray of 1332.4 keV ^{60}Co gamma-ray and efficiency of 32%. Energy calibration of the detector was performed using ^{152}Eu. Certified uranium and thorium standards of 10 µg/g were prepared from Inorganic Ventures. Certified reference materials from the National Institute of Standards and Technology (NIST) were used for quality control measurements. The NAA values were in excellent agreement with the NIST values as seen in Table 3.

Table 2: Irradiation and decay information

Nuclide	Technique	Power	Irradiation time	Decay time	Counting time
^{238}U	Epithermal	500 kW	2 min	10 min	5 min
^{232}Th	Thermal	950 kW	3 h	2 weeks	4 h

Table 3: NAA results as compared to NIST certified values

	NAA results	NIST certified values
1632d coal	1.43 ± 0.05 µg/g (Th)	1.428 ± 0.035 µg/g (Th)

1633c fly ash	23.8 ± 0.8 µg/g (Th)	23.0 ± 0.4 µg/g (Th)
1632d coal	0.502 ± 0.019 µg/g (U)	0.517 ± 0.012 µg/g (U)
2709a soil	3.09 ± 0.11 µg/g (U)	3.15 ± 0.05 µg/g (U)

209

210 The overall uncertainties for the samples and standards were the counting statistics for the uranium
211 and thorium standards, the uncertainties in the concentrations and counting statistics for the
212 samples of certified reference materials all taken in quadrature. For all measured NOR, the values for
213 A_f were corrected for mass loss during leaching. The criteria for release of NOR to groundwater are
214 specified in the Euratom Drinking Water Directive 2013/51/Euratom (Council of the European Union,
215 2013).

216

217 **2.5 Analysis procedure for non-radiological elements**

218 The leaching of non-radiological elements was assessed as a function of L/S (7 eluate fractions) using
219 an inductively coupled plasma optical emission spectrometer (ICP-OES, Perkin Elmer Optima 8300,
220 RSD < 2%) for analysis of Al, Ca, Fe, K, Mg, Na, P, Pb, S and Si, and ion-chromatography (IC, Dionex
221 DX120) for analysis of Cl and F. For IC, an analytical column (IonPac AS14A) with a conductivity
222 detector was used, and the pH of the eluates was buffered using 1 mM $NaHCO_3$ (supplied by Merck)
223 and 8 mM Na_2CO_3 (supplied by Merck). The detection limits (DL) for the quantification of given
224 elements are shown in Table 4.

225 **Table 4**: DL for ICP-OES (Al, Ca, Fe, K, Mg, Na, P, Pb, S and Si) and IC (Cl and F)

Element	Al	Ca	Fe	K	Mg	Na	P	Pb	S	Si	Cl	F
DL (in mg/l)	< 0.1	< 0.1	< 0.5	< 7	< 0.1	< 1	< 1	< 0.5	< 5	< 0.5	0.1	1

226

227 **2.6 Mercury intrusion porosimetry**

Mercury intrusion porosimetry (MIP) was applied on samples after 28 days of curing. After their curing period, samples were dried at 40 °C in a laboratory oven till constant mass, whereafter they were cooled down in a desiccator. MIP was governed by the Washburn-Laplace equation (Cook and Hover, 1993; Washburn, 1921):

$$P = \frac{4\gamma cos\theta}{d} \quad (Eq.2)$$

where P is the mercury injection pressure (Pa), γ is the surface tension of mercury (N/m), θ is the contact angle between solid and mercury (°), and d is the pore access diameter (m). The tests were performed with a Micromeritics Autopore IV 9500 V1.07 mercury porosimeter with a maximum injection pressure of 207 MPa. By assuming a contact angle of 130° and a mercury surface tension of 485 x 10^{-3} N/m, the minimum pore access diameter reached is about 6 x 10^{-9} m.

3. Results and discussion

3.1 Leaching of naturally occurring radionuclides

The leaching of NOR was assessed by means of gamma spectroscopy (^{226}Ra, ^{210}Pb, ^{228}Ra and ^{40}K) and NAA (^{238}U and ^{232}Th) by radiometrically counting the samples before (A_0) and after (A_f) leaching with a cumulative L/S of 10.0 ± 0.5 l/kg. An overview of the results is shown in Table 5.

Table 5: A_0 and A_f (in Bq/kg) for ^{238}U, ^{226}Ra, ^{210}Pb, ^{232}Th, ^{228}Ra and ^{40}K

		^{238}U	^{226}Ra	^{210}Pb	^{232}Th	^{228}Ra	^{40}K
Sample 1	A_0	65.2 ± 0.9	125.9 ± 5.7	67.0 ± 9.9	32.7 ± 0.5	30.4 ± 1.1	79.8 ± 3.6
	A_f	76.5 ± 1.1	129.3 ± 2.8	69.0 ± 10.1	26.2 ± 0.2	32.1 ± 1.2	45.4 ± 2.5
Sample 2	A_0	75.8 ±	136.2 ±	68.1 ±	32.6 ±	32.6 ±	88.7 ±

		1.2	6.2	10.1	0.7	1.2	4.0
	A_f	82.0 ± 1.2	140.7 ± 6.4	68.6 ± 10.1	29.3 ± 0.2	32.6 ± 1.2	21.5 ± 2.1
Sample 3	A_0	72.2 ± 1.1	129.2 ± 5.8	65.3 ± 9.6	33.2 ± 0.5	30.9 ± 1.1	77.5 ± 3.5
	A_f	77.5 ± 1.1	133.7 ± 6.1	62.3 ± 9.2	27.9 ± 0.2	31.6 ± 1.2	22.8 ± 1.7

From Table 5, it can be observed that the activity concentrations for the NOR from the ^{238}U decay chain (i.e. ^{238}U, ^{226}Ra and ^{210}Pb) vary, indicating disequilibrium (as a consequence of the enhanced ^{226}Ra concentration in PG). The ^{232}Th decay chain is assumed to be equilibrium since the activity concentrations of ^{232}Th and ^{228}Ra are equal. In general, the radionuclides from the ^{238}U decay chain show higher activity concentrations compared to the ones from the ^{232}Th decay chain. As a result of the up-flow percolation leaching test, the activity concentrations of ^{226}Ra, ^{210}Pb and ^{228}Ra remained the same (within the boundaries of their uncertainty) for all samples, while the activity concentrations of ^{238}U were slightly higher after leaching. It can be concluded that ^{238}U, ^{226}Ra, ^{210}Pb and ^{228}Ra were retained very well in the solid matrix. For all samples, both for ^{232}Th and ^{40}K, a decrease in activity concentration was observed due to leaching, indicating that these nuclides left the solid matrix. In Fig. 1, the release (in %) of NOR, calculated with Eq. 1, is shown.

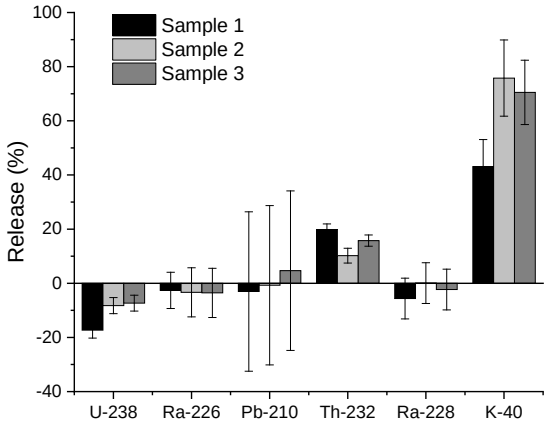

257

258 **Figure 1**: Release of NOR as a consequence of leaching

259 The release of ^{232}Th was highest for sample 1 (19.9 ± 2.0%), while it was lowest for sample 2 (10.2 ±
260 2.7%). For sample 3, release of ^{232}Th was 15.8 ± 2.1%. For ^{40}K, the opposite was observed, with the
261 highest release for samples synthesized with a sodium hydroxide solution (75.8 ± 14.1% for sample 2
262 and 70.5 ± 11.9% for sample 3), while the use of a sodium silicate solution resulted in lowest ^{40}K
263 release (i.e. 43.1 ± 10.0%).

264 Although ^{232}Th and ^{238}U are both actinides, ^{238}U was not released upon leaching. There is only limited
265 published data on the solubility of actinides in cementitious pore waters, which concentrates mostly
266 on the effect of additives, e.g. EDTA or plasticizers (Colàs et al., 2013; Kitamura et al., 2013).
267 Regarding the binding mechanisms of actinides to cement, less information exists on thorium,
268 compared to uranium (Evans, 2008). Thorium has a very stable tetravalent oxidation state (Choppin
269 et al., 2001), while uranium is expected to exist in the form of U^{6+} in an alkaline environment (Evans,
270 2008). Most likely, thorium forms leachable and non-leachable complexes with other chemical
271 species upon alkali activation. In aqueous media, thorium is almost always present as Th^{4+} (Rand et
272 al., 2008) and in alkaline solutions thorium is expected to form thorium hydroxide complexes
273 ($Th_m(OH)_{4m}$) (Rand et al., 2008). Also, high pH values give rise to carbonates, resulting in the
274 formation of mixed thorium-hydroxo-carbonate complexes and thorium carbonate complexes

(Altmaier et al., 2005, 2006). Several other chemical species are available for complexation, of which all of them show different thermodynamic properties. There is no evidence for complex formation between Th^{4+} and ClO_4^-, while Th^{4+} forms strong complexes with fluoride (with stoichiometry ThF_n^{4-n}, with n from 1 to 6) (Rand et al., 2008). The formation of species like $Th(SO_4)_n^{4-2n}$ (with n from 1 to 4) is also reasonable because of their very high solubility (Rand et al., 2008). However, the extent to which expected thorium complexes are formed is out of the scope of this research paper. Since thorium leaching was highest for sample 1, the use of a sodium silicate solution gives rise to the formation of more leachable thorium complexes, compared to sodium hydroxide activated samples.

Upon alkali activation, the formation of uranium-mineral phases is responsible for its retention in the solid phase. This was already demonstrated in several studies on cementitious materials (Matzen et al., 2000; Sutton et al., 2003), wherein uranium gets adsorbed to silicate surfaces (Sylwester et al., 2000; Tits et al., 2015) and incorporated into the C-S-H (calcium-silicate-hydrate) structure (Felipe-sotelo et al., 2017; Tits et al., 2015), limiting its solubility. Due to the incorporation of PG containing remnants of phosphoric acid, the formation of uranium-phosphate phases may be evident, which were also demonstrated in cement (Wellman et al., 2007). Highest release was observed for potassium, which acts as charge-balancing ion at the negatively charged silicate surface sites (Tänzer et al., 2017). Since potassium belongs to the group of salts, it shows pH independent leaching. Furthermore, as discussed in section 3.2, potassium shows the same leaching behavior as sodium. The release of potassium and sodium is higher for sodium hydroxide activated samples, because their excessiveness was higher compared to sample 1. Radium and lead were retained very well. Since radium is chemically very similar to calcium, a multiphase immobilization is expected, as explained in (Gijbels et al., 2018). The immobilization of lead is due to its precipitation as $Pb(OH)_2$ in the solid structure (Koplík et al., 2016).

The leaching of the different isotopes is affecting the destiny of thorium itself or its daughters to very different degrees. Since the long living isotopes ^{232}Th ($t_{1/2}$ = 14 10^9 y) and ^{230}Th ($t_{1/2}$ = 75.4 10^3 y) are

chemically the same elements, their leaching behavior is expected to be similar. Leaching of ^{230}Th can have influence on the equilibria in its respective decay chain, and will in the very long term result in enhanced concentrations of ^{226}Ra and progeny in soil and soil water. Since ^{232}Th is the primordial element of its decay chain, its leaching behavior will not give rise to disequilibria, but in the long term lead to slightly lower activity concentrations for all its daughters in the building material.

Referring to the European Drinking Water Directive (Council of the European Union, 2013), none of the NOR considered (i.e. ^{238}U, ^{234}U, ^{226}Ra, ^{228}Ra, ^{210}Pb and ^{210}Po) leached out from the solid AAM matrix. At first glance, drinking water is not endangered. However, the ^{226}Ra concentration in soil and soil water is likely to increase as a consequence of ^{230}Th leaching. ^{210}Pb (and consequently ^{210}Po) concentrations are not expected to be of concern because ^{210}Pb was retained in the solid matrix and the half-life of ^{226}Ra is 1600 y. However, the extent to which concentrations will rise or decline, requires advanced modeling, and is also influenced by geochemical and biological processes occurring during the life-time of AAMs. Also, additional alpha- and beta spectroscopy are desirable to confirm the statements about ^{210}Pb and ^{210}Po, respectively.

3.2 Leaching of non-radiological elements

The leaching of non-radiological elements was assessed by means of ICP-OES and IC as a function of L/S. For Fe, Mg, P and Pb the concentrations in the eluates were below the detection limits (see Table 4). The change in pH during the column experiments is illustrated in Fig. 2. The general trends in eluate pH were similar for all samples. Initially, the pH increased during the first 2 fractions, followed by a decrease from approximately 13.4 to 12.6. The pH increase is attributed to the dissolution of alkaline elements, such as sodium and potassium, and sulphate (SO_4^{2-}). There is no doubt that the eluate pH will decrease with increasing L/S.

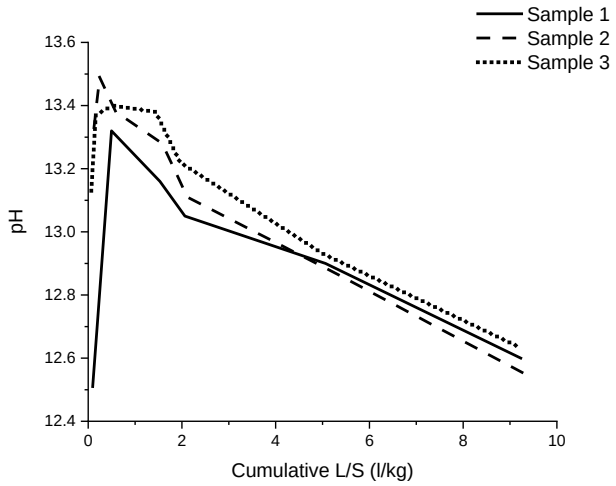

323

324 **Figure 2**: Eluate pH as a function of cumulative L/S

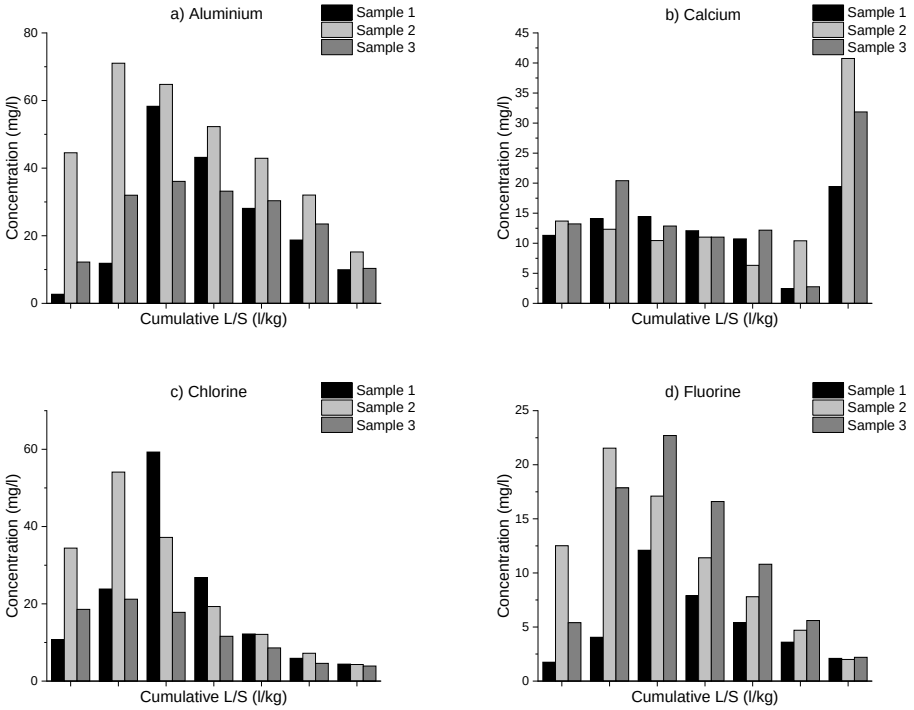

325

326

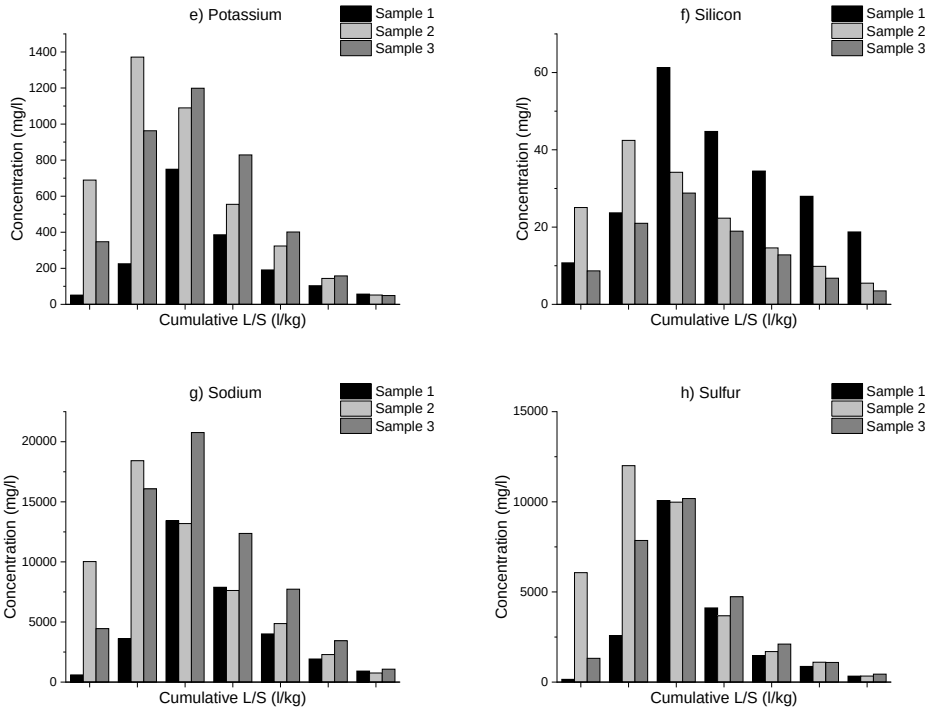

Figure 3: Concentration as a function of cumulative L/S for a) aluminium, b) calcium, c) chlorine, d) fluorine, e) potassium, f) silicon, g) sodium and h) sulfur

Fig. 3 reports the concentrations (in mg/l) as a function of cumulative L/S for Al, Ca, Cl, F, K, Si, Na and S. The release of Fe, Mg, P and Pb is not shown because neither of the eluates contained measurable concentrations of these elements. Looking at the results reported in Fig. 3, it can be noticed that the trends of mass release for the different samples are quite similar. This reveals on the one hand a similar behavior of the samples, and on the other hand, a good reproducibility of the column test and the consistency of leaching data. The release mechanisms for the measurable elements were investigated in order to predict the long term release of these during the use scenario as well as end-of-life phases of the AAM. Ca shows a different release mechanism compared to the other elements investigated, which also remained unidentified following CEN/TS 16637-3. Al, Cl, F, K, Si, Na and S show pH dependent solubility controlled release.

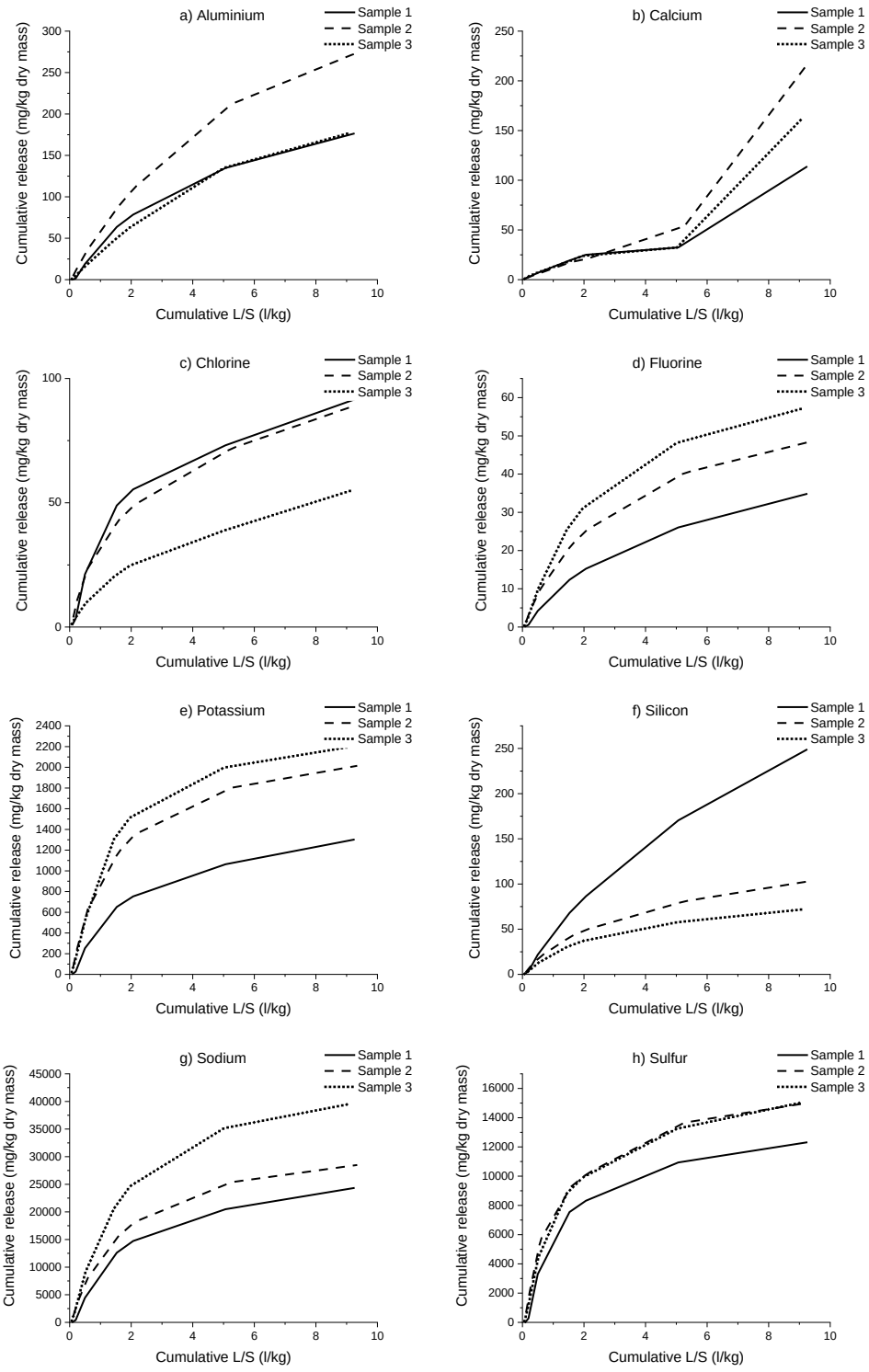

Figure 4: Cumulative release as a function of cumulative L/S for a) aluminium, b) calcium, c) chlorine, d) fluorine, e) potassium, f) silicon, g) sodium and h) sulfur

In Fig. 4, the cumulative release (in mg/kg dry mass) as a function of cumulative L/S for Al, Ca, Cl, F, K, Si, Na and S is depicted. It is clear that the use of different alkali activators substantially affected the

leaching capacity of the samples, although the evolution patterns were quite similar. The cumulative release of Al, Cl, F, K, Si Na and S increased progressively with respect to L/S. A sharp increase of Ca concentration in the eluates was observed for L/S 10.0 ± 0.5 l/kg. This behavior can be attributed to the sequential mode of leaching, where initially the depletion of SO_4^{2-} occurs and Ca mobility is impeded, whereafter Ca transport is facilitated. The use of a sodium silicate solution resulted in highest cumulative release of Si, while Na and K release were highest in case of sodium hydroxide solutions, indicating that these elements were in excess. More Al was leached when the H_2O content in the alkali activator was higher. Cl was immobilized better when a sodium hydroxide solution was used, while the opposite trend was observed for F for which sample 1 was the best performing immobilization matrix. The leaching of Cl and Si was higher for sample 1, which showed also the highest ^{232}Th release. However, it is expected that multiple leachable thorium complexes were formed, making it impossible to predict to which extent they individually contribute to ^{232}Th leaching in this case study.

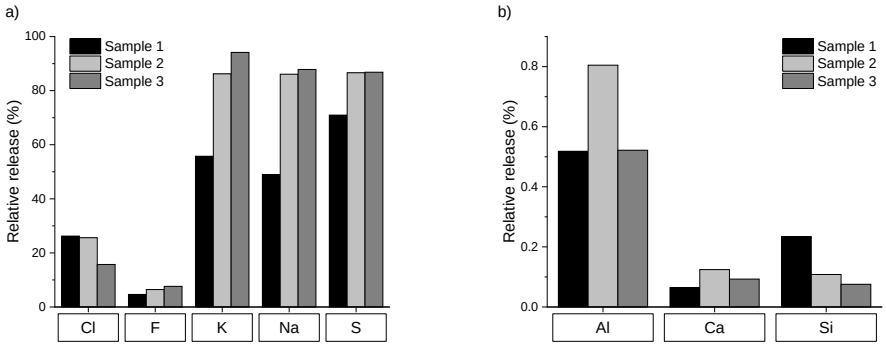

Figure 5: Relative release for a) chlorine, fluorine, potassium, sodium and b) aluminium, calcium and silicon

By comparing the cumulative release (in mg/kg dry mass) of each element provided by the column test (at cumulative L/S 10.0 ± 0.5 l/kg) with the total content, the relative release (in %) was calculated. Results are shown in Fig. 5. Only a small amount of Al, Ca and Si is mobilized, at least if the environmental conditions (pH, temperature, flow rate) are similar to the tested ones. In fact, the

release percentage was about 0.5 to 0.8% for Al, 0.1 to 0.2% for Ca and 0.1 to 0.3% for Si. The highest mobility was observed for K, Na and S with release percentages up to 56-94%, 49-88% and 71-87%, respectively. During the hydration process, some K and Na may have been replaced by Ca. Lowest release for K, Na and S was observed for sample 1. Release of Cl was 16-26% and for F was 4-8%. Except for S, the elements originating from PG (i.e. Ca, Cl and F) are fairly well retained in the AAM structure, which is good from the environmental point of view. Since the relative release of Na and S are similar for sample 2 and sample 3, it is expected that the excessive amounts of Na resulted in soluble thenardite formation.

In the long term, it is expected that the pH generally will decrease to neutral, and the release of constituents will decline. However, it is worth pointing out that long-term field predictions based on these results should be treated with caution since it neglects different geochemical and biological processes which are likely to occur during the life-time of the AAMs, and that can significantly influence the release. Considering the European Drinking Water Directive (Council of the European Union, 2013), the non-radiological elements of concern in this particular case are Al, Cl, F, Na and S, for which modelling and monitoring is required in case these AAMs are used in the immediate vicinity of a drinking water supply. It is also important to note that the pH of drinking water should be lower than 9.5.

3.3 Mercury intrusion porosimetry

The results from MIP are shown in Fig. 6 and Fig. 7. From Fig. 6, it is observed that the final intruded pore volumes for sample 2 and sample 3 are almost double the volume intruded for sample 1. Also the total pore area was much larger for samples activated with sodium hydroxide. The highest H_2O/Na_2O in the alkali activator (i.e. sample 2) led to highest total intrusion volume and total pore area (0.22 ml/g and 19 m^2/g, respectively). The data comply with those found by (Nedeljkovíc et al., 2018; Park et al., 2014) on alkali-activated GGBFS.

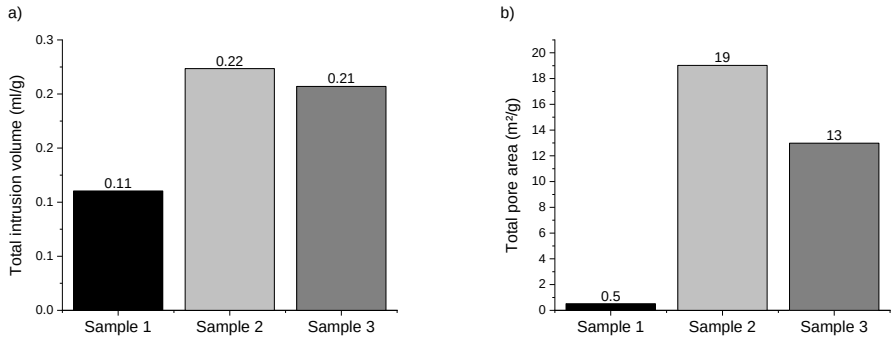

Figure 6: a) Total intrusion volume and b) total pore area

In Fig. 7 the cumulative pore volume distribution is shown. The pore size distribution of sample 2 and sample 3 are similar, while the curve shape of sample 1 is quite different. Sample 1, activated with a sodium silicate solution, shows a higher amount of pores with diameters in the range of 1 µm to 100 µm, compared to the other samples. In the range from 10 nm to 1 µm, there is almost no increase in pore volume for sample 1, resulting in lowest cumulative pore volume. The use of a sodium hydroxide solution increases the cumulative pore volume, with highest amount of pores in the range from 10 nm to 300 nm. A higher H_2O/Na_2O for a sodium hydroxide solution (i.e. sample 2) gives rise to a lower amount of pores in the range from 100 nm to 100 µm, but a higher amount of pores in the range from 10 nm to 100 nm, compared to sample 3.

For most investigated elements (i.e. ^{40}K, Al, Ca, F, K, Na and S), a lower pore volume and pore surface area of the AAM results in lowest release upon leaching, which was the case for sample 1 activated with a sodium silicate solution. On the contrary, the release of ^{232}Th, Cl and Si was higher for sample 1. It can be concluded that both the porosity and formation of multiple leachable and non-leachable complexes are determining factors for the release of elements from AAMs. Further investigation of the formed complexes upon alkali activation is needed to validate the hypothesis and further investigate the influence of alkali activator.

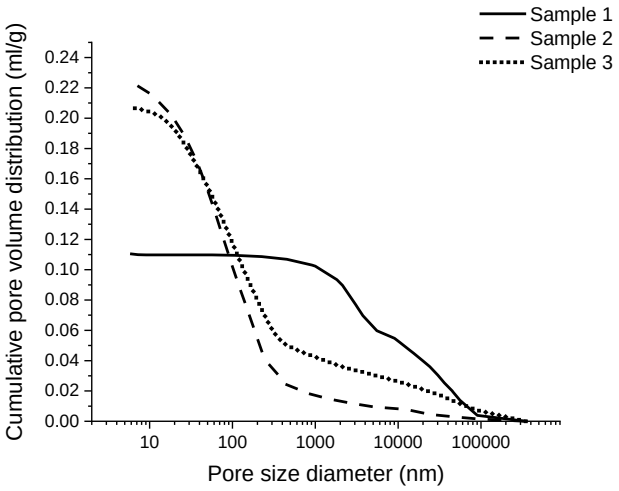

412

413 **Figure 7**: Cumulative pore volume distribution

414

415 **4. Conclusions**

416 Leaching of NOR and inorganic non-radiological elements from AAMs based on GGBFS when PG was
417 incorporated, was assessed. It is concluded that ^{238}U, ^{226}Ra, ^{210}Pb, and ^{228}Ra were retained very well.
418 Both for ^{232}Th and ^{40}K, a decrease in activity concentration was observed due to leaching and their
419 release was influenced by the use of different alkali activators. The use of a sodium silicate solution
420 gave rise to the highest ^{232}Th leaching (19.9 ± 2.0%), while the use of sodium hydroxide solutions
421 resulted in the highest ^{40}K release (75.8 ± 14.1% and 70.5 ± 11.9%). Also the leaching of non-
422 radiological elements was affected by the use of different alkali activators. In general, only a small
423 amount of Al (0.5-0.8%), Ca (0.1-0.2%) and Si (0.1-0.3%) was mobilized, while the highest release was
424 observed for K (56-94%), Na (49-88%) and S (71-87%). ^{40}K showed the same leaching behavior as K
425 and Na, while for ^{232}Th it was concluded that the formation of multiple leachable thorium complexes
426 was responsible for its release. The extent to which these complexes individually contribute to
427 leaching, and the influence of the alkali activator on their formation, forms a subject of further study.
428 At first glance, drinking water is not endangered by leaching of NOR following the requirements of
429 the European Drinking Water Directive. The non-radiological elements of concern in this regard are

Al, Cl, F, Na and S, for which modelling and monitoring is required in case these AAMs are used in the immediate vicinity of a drinking water supply. Also the pH should be monitored, since its value should not exceed 9.5 for drinking water purposes. From the MIP results, it was concluded that both the porosity and formation of multiple leachable and non-leachable complexes are determining factors for the release of elements from AAMs.

Acknowledgements

This work was supported by the fund for scientific research Flanders (FWO), and hosted by the University of Hasselt, the KU Leuven and the University of Texas. The authors would like to thank Jenny Put for the IC measurements and to acknowledge the networking support of the COST Action TU1301, www.norm4building.org.

References

Altmaier, B.M., Neck, V., Müller, R., Fanghänel, T., 2005. Solubility of ThO2·xH2O(am) in carbonate solution and the formation of ternary Th(IV) hydroxide-carbonate complexes. Radiochim. Acta 93, 83–92. https://doi.org/10.1524/ract.93.2.83.59420

Altmaier, M., Neck, V., Denecke, M.A., Yin, R., Fanghänel, T., 2006. Solubility of ThO2·xH2O(am) and the formation of ternary Th(IV) hydroxide-carbonate complexes in NaHCO3-Na2CO3 solutions containing 0-4 M NaCl. Radiochim. Acta 94, 495–500. https://doi.org/10.1524/ract.2006.94.9-11.495

ASTM International, 2017. ASTM C204-17. Standard test methods for fineness of hydraulic cement by air-permeability apparatus.

Bureau voor Normalisatie (NBN), 2010. EN 196-6. Methods of testing cement - Part 6: Determination of fineness.

Cappuyns, V., Swennen, R., 2008. The use of leaching tests to study the potential mobilization of heavy metals from soils and sediments: A comparison. Water. Air. Soil Pollut. 191, 95–111. https://doi.org/10.1007/s11270-007-9609-4

Central Pollution Control Board, 2012. Guidelines for management and handling of phosphogypsum generated from phosphoric acid plants (Final Draft). Delhi.

Choppin, G.R., Liljenzin, J.-O., Rydberg, J., 2001. Radiochemistry and nuclear chemistry, 3rd ed. Elsevier Science & Technology, Woburn.

461 Colàs, E., Grivé, M., Rojo, I., Duro, L., 2013. The effect of gluconate and EDTA on thorium solubility
462 under simulated cement porewater conditions. J. Solution Chem. 42, 1680–1690.
463 https://doi.org/10.1007/s10953-013-0054-2

464 Contreras, M., Gázquez, M.J., García-Díaz, I., Alguacil, F.J., López, F.A., Bolívar, J.P., 2013. Valorisation
465 of waste ilmenite mud in the manufacture of sulphur polymer cement. J. Environ. Manage. 128,
466 625–630. https://doi.org/10.1016/j.jenvman.2013.06.015

467 Contreras, M., Martín, M.I., Gázquez, M.J., Romero, M., Bolívar, J.P., 2014. Valorisation of ilmenite
468 mud waste in the manufacture of commercial ceramic. Constr. Build. Mater. 72, 31–40.
469 https://doi.org/10.1016/j.conbuildmat.2014.08.091

470 Cook, R.A., Hover, K.C., 1993. Mercury porosimetry of cement-based materials and associated
471 correction factors. Constr. Build. Mater. 7, 231–240. https://doi.org/10.1016/0950-
472 0618(93)90007-Y

473 Council of the European Union, 2014. Council directive 2013/59/EURATOM, European Basic Safety
474 Standards (BSS) for Protection against Ionising Radiation. Off. J. Eur. Union L 13/1.

475 Council of the European Union, 2013. European drinking water directive 2013/51/EURATOM, laying
476 down requirements for the protection of the health of the general public with regard to
477 radioactive substances in water intended for human consumption. Off. J. Eur. Union L 296/12.

478 Croymans, T., Leonardi, F., Trevisi, R., Nuccetelli, C., Schreurs, S., Schroeyers, W., 2017. Gamma
479 exposure from building materials - A dose model with expanded gamma lines from naturally
480 occurring radionuclides applicable in non-standard rooms. Constr. Build. Mater. 159, 768–778.
481 https://doi.org/10.1016/j.conbuildmat.2017.10.051

482 European Committee for Standardization, 2016. CEN/TS 16637-3. Construction products: Assessment
483 of release of dangerous substances - Part 3: Horizontal up-flow percolation test.

484 Evans, N.D.M., 2008. Binding mechanisms of radionuclides to cement. Cem. Concr. Res. 38, 543–553.
485 https://doi.org/10.1016/j.cemconres.2007.11.004

486 Felipe-sotelo, M., Hinchliff, J., Field, L.P., Milodowski, A.E., Preedy, O., Read, D., 2017. Retardation of
487 uranium and thorium by a cementitious backfill developed for radioactive waste disposal.
488 Chemosphere 179, 127–138. https://doi.org/10.1016/j.chemosphere.2017.03.109

489 Gijbels, K., Ion Iacobescu, R., Pontikes, Y., Vandevenne, N., Schreurs, S., Schroeyers, W., 2018. Radon
490 immobilization potential of alkali-activated materials containing ground granulated blast
491 furnace slag and phosphogypsum. Constr. Build. Mater. 184, 68–75.
492 https://doi.org/10.1016/j.conbuildmat.2018.06.162

493 Hjelmar, O., Wahlström, M., Comans, R., Kalbe, U., Grathwohl, P., Mehu, J., Schiopu, N., Hykš, J.,
494 Laine-ylijoki, J., van Zomeren, A., Krüger, O., Schoknecht, U., Wendel, T., Abdelghafour, M.,
495 Borho, N., 2012. Robustness validation of two harmonized European leaching tests for
496 assessment of the leaching of construction products, including waste-based construction
497 materials, in: WASCON 2012 Gothenburg, Sweden. pp. 1–5.

498 Huang, X., Zhuang, R., Muhammad, F., Yu, L., Shiau, Y., Li, D., 2017. Solidification/stabilization of
499 chromite ore processing residue using alkali-activated composite cementitious materials.
500 Chemosphere 168, 300–308. https://doi.org/10.1016/j.chemosphere.2016.10.067

501 International Atomic Energy Agency (IAEA), 2013. Radiation Protection and Management of NORM
502 Residues in the Phosphate Industry, Safety Reports Series No. 78. IAEA, Vienna.
503 https://doi.org/10.1016/j.resourpol.2012.04.002

504 Kitamura, A., Fujiwara, K., Mihara, M., Cowper, M., Kamei, G., 2013. Thorium and americium

505 solubilities in cement pore water containing superplasticiser compared with thermodynamic
506 calculations. J. Radioanal. Nucl. Chem. 298, 485–493. https://doi.org/10.1007/s10967-013-
507 2618-4

508 Koplík, J., Kalina, L., Másilko, J., Šoukal, F., 2016. The characterization of fixation of Ba, Pb, and Cu in
509 alkali-activated fly ash/blast furnace slag matrix. Materials (Basel). 9.
510 https://doi.org/10.3390/ma9070533

511 Kuo, W.-T., Wang, H.-Y., Shu, C.-Y., 2014. Engineering properties of cementless concrete produced
512 from GGBFS and recycled desulfurization slag. Constr. Build. Mater. 63, 189–196.
513 https://doi.org/10.1016/j.conbuildmat.2014.04.017

514 Lancellotti, I., Catauro, M., Dal, F., Kiventer, J., Leonelli, C., Illikainen, M., 2018. Alkali activation as
515 new option for gold mine tailings inertization. J. Clean. Prod. 187, 76–84.
516 https://doi.org/10.1016/j.jclepro.2018.03.182

517 Matzen, S.L., Beiriger, J.M., Torretto, P.C., Zhao, P., Viani, B.E., 2000. Uranium (VI) and neptunium (V)
518 transport through fractured, hydrothermally altered concrete. Radiochim. Acta 88, 657–664.
519 https://doi.org/10.1524/ract.2000.88.9-11.657

520 Michalik, B., de With, G., Schroeyers, W., 2018. Measurement of radioactivity in building materials -
521 Problems encountered caused by possible disequilibrium in natural decay series. Constr. Build.
522 Mater. 168, 995–1002. https://doi.org/10.1016/j.conbuildmat.2018.02.044

523 Mossini, E., Macerata, E., Giola, M., Mariani, M., 2015. Review of international normatives for natural
524 radioactivity determination in building materials. Nukleonika 60, 597–602.
525 https://doi.org/10.1515/nuka-2015-0101

526 Nebel, H., Spanka, G., 2013. Harmonisation of test methods for the execution of the european
527 construction products directive (CPD). Validation of a european leaching test for construction
528 products. Waste and Biomass Valorization 4, 759–767. https://doi.org/10.1007/s12649-013-
529 9215-1

530 Nedeljkovíc, M., Šavija, B., Zuo, Y., Lukovic, M., Ye, G., 2018. Effect of natural carbonation on the pore
531 structure and elastic modulus of the alkali-activated fly ash and slag pastes. Constr. Build.
532 Mater. 161, 687–704. https://doi.org/10.1016/j.conbuildmat.2017.12.005

533 Nguyen, H., Adesanya, E., Ohenoja, K., Kriskova, L., Pontikes, Y., Kinnunen, P., Illikainen, M., 2018. By-
534 product based ettringite binder - A synergy between ladle slag and gypsum. Constr. Build.
535 Mater. Submitted.

536 Nuccetelli, C., Pontikes, Y., Leonardi, F., Trevisi, R., 2015. New perspectives and issues arising from
537 the introduction of (NORM) residues in building materials: A critical assessment on the
538 radiological behaviour. Constr. Build. Mater. 82, 323–331.
539 https://doi.org/10.1016/j.conbuildmat.2015.01.069

540 Park, J.W., Hong, S.I., Yang, H.J., Lima, T., Ann, K.Y., 2014. Cement-free mortar using ground
541 granulated blast-furnace slag with different alkali-activators. Appl. Mech. Mater. 578–579,
542 1430–1440. https://doi.org/10.4028/www.scientific.net/AMM.578-579.1430

543 Provis, J.L., 2017. Alkali-activated materials. Cem. Concr. Res. (In Press).
544 https://doi.org/10.1016/j.cemconres.2017.02.009

545 Rand, M.H., Mompean, F.J., Perrone, J., Illemassène, M., 2008. Chemical thermodynamics of thorium.
546 OECD Pub.

547 Rashad, A.M., 2017. Phosphogypsum as a construction material. J. Clean. Prod. 166, 732–743.
548 https://doi.org/10.1016/j.jclepro.2017.08.049

549 Sas, Z., Doherty, R., Kovacs, T., Soutsos, M., Sha, W., Schroeyers, W., 2017. Radiological evaluation of
550 by-products used in construction and alternative applications; Part I. Preparation of a natural
551 radioactivity database. Constr. Build. Mater. 150, 227–237.
552 https://doi.org/10.1016/j.conbuildmat.2017.05.167

553 Shakhashiro, A., Sansone, U., Wershofen, H., Bollhöfer, A., Kim, C.K., Kim, C.S., Kis-Benedek, G.,
554 Korun, M., Moune, M., Lee, S.H., Tarjan, S., Al-Masri, M.S., 2011. The new IAEA reference
555 material: IAEA-434 technologically enhanced naturally occurring radioactive materials
556 (TENORM) in phosphogypsum. Appl. Radiat. Isot. 69, 231–236.
557 https://doi.org/10.1016/j.apradiso.2010.09.002

558 Shi, C., Fernández-Jiménez, A., 2006. Stabilization/solidification of hazardous and radioactive wastes
559 with alkali-activated cements. J. Hazard. Mater. 137, 1656–1663.
560 https://doi.org/10.1016/j.jhazmat.2006.05.008

561 Sutton, M., Warwick, P., Hall, A., 2003. Uranium (VI) interactions with OPC/PFA grout. J. Environ.
562 Monit. 5, 922. https://doi.org/10.1039/b308554f

563 Sylwester, E.R., Hudson, E.A., Allen, P.G., 2000. The structure of uranium (VI) sorption complexes on
564 silica, alumina, and montmorillonite. Geochim. Cosmochim. Acta 64, 2431–2438.
565 https://doi.org/10.1016/S0016-7037(00)00376-8

566 Tänzer, R., Jin, Y., Stephan, D., 2017. Alkali activated slag binder: effect of cations from silicate
567 activators. Mater. Struct. Constr. 50. https://doi.org/10.1617/s11527-016-0961-y

568 Tayibi, H., Choura, M., López, F.A., Alguacil, F.J., López-Delgado, A., 2009. Environmental impact and
569 management of phosphogypsum. J. Environ. Manage. 90, 2377–2386.
570 https://doi.org/10.1016/j.jenvman.2009.03.007

571 Tits, J., Walther, C., Stumpf, T., Macé, N., Wieland, E., 2015. A luminescence line-narrowing
572 spectroscopic study of the uranium (VI) interaction with cementitious materials and titanium
573 dioxide. Dalt. Trans. 44, 966–976. https://doi.org/10.1039/c4dt02172j

574 Ulubeyli, G.C., Artir, R., 2015. Sustainability for blast furnace slag: Use of some construction wastes.
575 Procedia - Soc. Behav. Sci. 195, 2191–2198. https://doi.org/10.1016/J.SBSPRO.2015.06.297

576 Wang, L., Yu, K., Li, J., Tsang, D.C.W., Poon, C.S., Yoo, J., Baek, K., Ding, S., Hou, D., Dai, J., 2018. Low-
577 carbon and low-alkalinity stabilization/solidification of high-Pb contaminated soil. Chem. Eng. J.
578 351, 418–427. https://doi.org/10.1016/j.cej.2018.06.118

579 Washburn, E.W., 1921. Note on a method of determining the distribution of pore sizes in a porous
580 material. Proc. Natl. Acad. Sci. 7, 115–116.

581 Wellman, D.M., Mattigod, S. V., Arey, B.W., Wood, M.I., Forrester, S.W., 2007. Experimental
582 limitations regarding the formation and characterization of uranium-mineral phases in concrete
583 waste forms. Cem. Concr. Res. 37, 151–160. https://doi.org/10.1016/j.cemconres.2006.11.004

584